

---

# EXPERIMENTAL AND NUMERICAL STUDIES OF T-SHAPED FOOTINGS

---

NIHAT KAYA and MURAT ORNEK

---

## about the authors

Nihat Kaya  
Mustafa Kemal University,  
Department of Civil Engineering  
31200 Iskenderun / Hatay, Turkey  
E-mail: nihatkaya09@hotmail.com

Murat Ornek  
Mustafa Kemal University,  
Department of Civil Engineering  
31200 Iskenderun / Hatay, Turkey  
E-mail: mornek@mku.edu.tr

---

## abstract

*In addition to vertical axial loads, the footings of structures are often subjected to eccentric loads caused by the forces of earth pressures, earthquakes, water, wind, etc. Due to eccentric loading, the two edges settle by different amounts, causing the footing to tilt and then the pressure below the footing does not remain uniform. The T-shape is proposed as a footing shape for improving the bearing capacity of shallow footings against the action of eccentric loads. The vertical insertion of the rigid T-shaped footing, into the bearing soil, provides considerable resistance, against both of sliding and overturning, enough to regain the reduction in bearing capacity and increase in settlement. In this study, a series of experimental and numerical results from the ultimate loads and settlement of T-shaped footings are reported. A total of 48 model tests were conducted for investigating the effects of different parameters, such as the problem geometry and soil density. The problem geometry was represented by two parameters, the load eccentricity ( $e$ ) and the insertion depth ( $H$ ) of the T-shape into the loose and dense sand soil. After the experimental stage, the numerical analyses were carried out using a plane strain, two-dimensional, finite-element-based computer program. The behaviour of the T-shape footing on sand beds is represented by the hardening soil model. The results of the experimental and numerical studies proved that the ultimate bearing capacity of a footing under eccentric loads could be improved by inserting*

*a vertical central cut-off rigidly connected to the footing bottom. The load settlement curves indicate that the higher load eccentricity results in a decrease in the bearing capacity of the strip footing. It was also proved that the ultimate bearing capacity values can, depending on the soil density, be improved by up to four times that of the loose sand case. This investigation is considered to have provided a useful basis for further research, leading to an increased understanding of the T-shaped footing design.*

---

## keywords

model test, finite-element method, T-shaped footing, eccentric loading, sand

---

## 1 INTRODUCTION

Shallow footings are used to carry different types of structures. These structures may transfer concentric or eccentric loads to their footings, according to the acting case of the loading. Apart from the vertical axial loads, the footings of portal framed buildings are often subjected to eccentric loads caused by the forces of earth pressures, earthquakes, water, wind, etc. Sometimes the corner of the column of these portal-framed buildings is located very close to the property line, and hence subjected to eccentric loading. The eccentricity in a strip footing,  $e$ , is defined as the ratio of the moment ( $M$ ) to the vertical load ( $Q$ ). For designing footings subjected to earthquake forces, adopting appropriate values of the horizontal and vertical seismic coefficients, equivalent seismic forces can be conveniently evaluated. These forces in combination with static forces make the foundations subjected to eccentric and/or eccentric-inclined loads. The problems of footings subjected to eccentric loads are frequently encountered by an engineer in the case of the footings of the retaining wall, abutments, columns, stanchions, portal framed buildings, etc. Due to eccentric loading, the two edges settle by different amounts, causing the footing to tilt and the pressure

below the footing does not remain uniform. The amount of tilt and the pressure at the base depend on the value of the eccentricity width ratio.

The T-shape is a footing shape used to improve the bearing capacity of shallow footings against the action of eccentric loads. In addition to the vertical settlement, eccentrically loaded footings may also be affected from both horizontal displacement (and sliding) and/or rotation (or overturning), which are reasons that can reduce the ultimate bearing capacity and increase the settlement. The vertical insertion of the proposed rigid T-shaped footing, into the soil, provides considerable resistance, against both sliding and overturning, enough to regain the reduction in bearing capacity and the increase in settlement.

Experimental, numerical and theoretical studies of the bearing capacity of differently shaped footings under an eccentric load have been carried out by many researchers in the past. Patra et al. [1] conducted laboratory model tests to determine the ultimate bearing capacity of an eccentrically loaded strip foundation supported by geogrid-reinforced sand. Based on the laboratory test results, an empirical relationship, called the reduction factor, was suggested that correlates the ratio of the ultimate bearing capacity of an eccentrically loaded foundation with that for a foundation where the load is applied centrally. It is reported that the reduction factor is a function of the foundation depth and eccentricity. Singh et al. [2] presented the result of the laboratory model tests on the effect of soil confinement on the behaviour of a model footing resting on Ganga sand under an eccentric-inclined load. The results indicate that the ultimate bearing capacity of the square footing can be appreciably increased by soil confinement under axial load as well under an eccentric-inclined load. It has been observed that such a confinement resists the lateral displacement of the soil underneath the footing, leading to a significant decrease in the vertical settlement and hence improving the ultimate bearing capacity. Saleh et al. [3] performed tests with skirted foundations, in which a vertical or inclined wall surrounds one or more sides of the soil mass beneath the footing that is one of the recognized bearing capacity improvement techniques. Various load inclination angles, load eccentricities and skirt lengths were investigated. They found that sliding resistance is the most critical factor in the overall stability of the flat strip footing subjected to a high load inclination angle. Increasing the skirt inclination angle increases the ultimate bearing capacity and decreases the corresponding settlement. The rate of improvement increases with the increase of the load inclination angle. Sadoglu et al. [4] performed a series of tests with an eccentrically loaded model surface shallow strip footing

on reinforced, dense sand to investigate the decrease of the ultimate loads with increasing eccentricity. It is shown that the ultimate load decreases with increasing eccentricity. Joshi and Mahiyar [5] presented a new type of foundation that is very useful under the eccentric inclined loading conditions. The Angle Shaped Footing under the eccentric inclined load has been observed. This was after conducting a series of experiments and verifying the experimental results with the Ansys package that is based on the Finite-Element Technique. It has been observed that the angle-shaped footing becomes more effective when the angle of the projection with the vertical is in the range 150 to 300. The horizontal displacements in the footing due to the inclined eccentric loading are also reduced to large extent and have been found to be a maximum up to 1 to 2% of the width of the foundation. Musso and Ferlisi [6] investigated the behaviour of a model strip footing, resting on a saturated dense sandy soil, subjected to centred or eccentric vertical loading. Experimental tests, carried out on a small-scale physical model, are able to reproduce the effective stress levels equivalent to those prevailing in the prototype problems. The collapse mechanism is formed either by one or two sliding surfaces, depending on both the load eccentricities and the hydraulic gradient values. Significant differences were shown to occur between the centred and the eccentric loading footing response. Nawghare et al. [7] investigated the bearing capacity of the eccentrically loaded footing. Testing for the bearing capacity of the centrally loaded footing and then for the eccentrically loaded footing with a different  $e/B$  ratio was carried out. For every footing the bearing capacity and the settlement were found for the central as well as the eccentric loading. These results of the central and eccentric loading are compared with each other for the same footing. The results of the different footings are also compared for the central and eccentric loading. It is found that for the rectangular footing, as the size of the footing increased the bearing capacity has increased in the cases of the footing loaded centrally and the eccentrically loaded footings. For a square footing it is observed that there is no large difference in the bearing capacity of the footing for the central load ( $e/B=0$ ) as well as in the eccentric loads, but a considerable difference is observed in the settlement of the footing. There are also researchers who studied the eccentric loading as numerical and theoretical perspectives. These include Taibeat and Carter [8], Taibeat and Carter [9], Hjiat et al. [10], Saran et al. [11] and Loukidis et al. [12]. Loukidis et al. [12] used the finite-element method for the determination of the collapse load of a rigid strip footing placed on a uniform layer of purely frictional soil subjected to inclined and eccentric loading. The footing was set on the free surface of the soil mass

with no surcharge applied. The soil was assumed to be elastic–perfectly plastic, following the Mohr–Coulomb failure criterion. Analyses for the associated and non-associated flow rules yielded essentially the same trends regarding the effective width, the inclination factor and the normalized vertical force–horizontal force–moment failure envelope. The results showed that the inclination factor depends on the value of the friction angle, whereas the effective width does not. Srinivasan and Ghosh [13] investigated the interaction between two nearby surface circular footings by conducting a number of laboratory-scale model tests on a dry, cohesionless Ennore sand bed. The interference effect between two closely spaced circular footings is obtained. They concluded that the bearing capacity of a single isolated footing on a double-layer soil deposit decreases with an increase in the depth of the top weak layer and a significant change in the bearing capacity and the settlement of the interfering footing is observed in a single- as well as double-layer soil deposit. Veiskarami and Kumar [14] computed the ultimate bearing capacity of strip foundations subjected to a horizontal groundwater flow using the stress-characteristics method. A numerical solution has been proposed both for smooth and rough footings placed on frictional soils. They found that the magnitude of  $f_y$  reduces continuously with an increase in the value of  $i$ . For a given hydraulic gradient, the value of  $f_y$  was found to reduce further with a decrease in the value of  $\Phi$ . He [15] conducted a series of computational modelings using the mesh-free local Petrov-Galerkin (MLPG) method to evaluate the bearing capacity and response behaviour of extended-length piles. It is concluded that the MLPG gives better accuracy in the results and the optimal length of the pile is directly related to the stiffness of the soil, when compared to the finite-element method. Dash [16] performed a series of model tests to develop an understanding of the influence of the geo-cell material on the load-carrying mechanism of the geo-cell-reinforced sand foundations under strip loading. It is concluded that the performance of the reinforced-sand foundation bed is influenced by the strength, stiffness, aperture-opening size and the orientation of the rib of the geo-cell material.

In this study, experimental and numerical investigations into the ultimate loads of T-shaped footings are reported. A total of 48 model tests in two different series was carried out using the facility in the Geotechnical Laboratory of the Civil Engineering Department of the Mustafa Kemal University, Iskenderun, Hatay, Turkey. The effect of eccentricity and the effect of the insertion depths under vertical loadings were investigated in Series I and Series II, respectively. The experimental and numerical studies in every series were performed both for the loose

and the dense sand conditions. The problem geometry was presented using two parameters, the load eccentricity ( $e$ ) and the insertion depth ( $H$ ) of the T-shape footing into the loose and the dense sand soils. The findings will help in a better understanding of the T-shaped footings design with a different soil density and with a different footing geometry. It is expected that the information presented in this study will provide a contribution to the literature results and will be an alternative source for the design and applications for geotechnical engineers. This will result in a decrease in the cost of construction and save simplicity and time for the engineer, the contractor and the owner of the construction.

## 2 EXPERIMENTAL INVESTIGATIONS

### 2.1 GENERAL

The experimental program was carried out using the facility in the Geotechnical Laboratory of the Civil Engineering Department of the Mustafa Kemal University, Iskenderun, Hatay, Turkey. The facility and a typical model are shown in Figures 1 and 2.

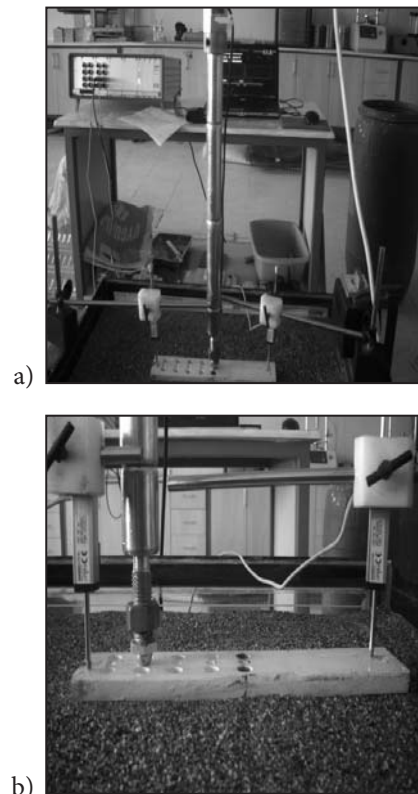


Figure 1. Test set-up: (a) overview; (b) footing.

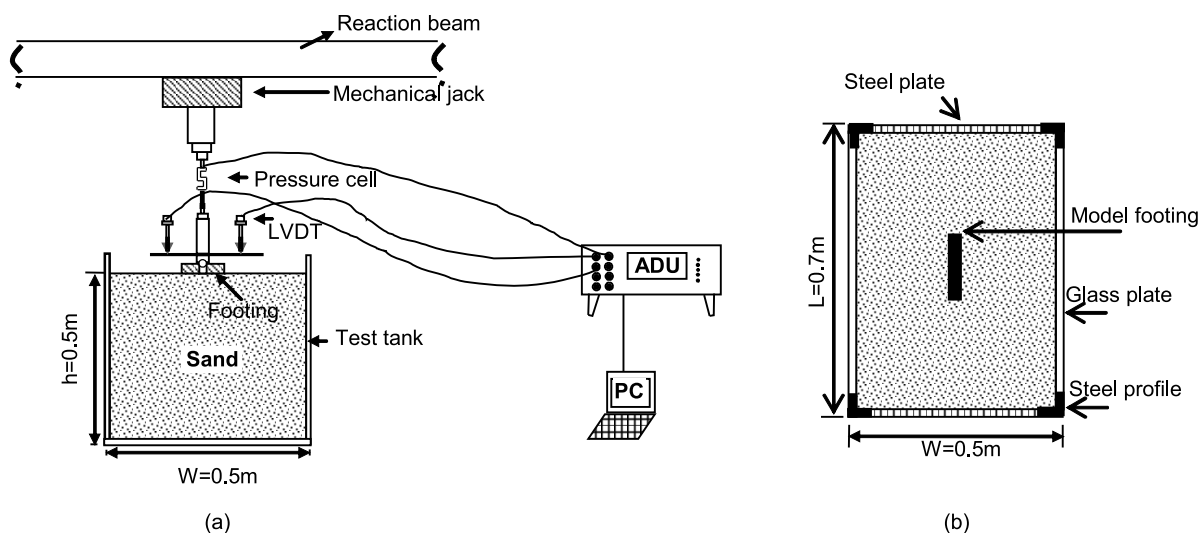


Figure 2. General layout of apparatus for the model test: (a) elevation; (b) plan view.

## 2.2 SOIL PROPERTIES

Uniform, clean, fine sand obtained from the Ceyhan River bed was used for the model tests. The laboratory tests were conducted on representative sand samples for the gradation, specific gravity, maximum and minimum densities and strength parameters. These properties are summarized in Table 1. The particle size distribution of this sand is shown in Figure 3. The model tests were conducted on loose sand and dense sand conditions. The angle of shearing resistances of the loose ( $D_r=25\%$ ) and dense sand ( $D_r=75\%$ ) at dry unit weights of  $16.65\text{kN/m}^3$  and  $17.11\text{kN/m}^3$  for normal pressures of 50, 100 and 200kPa were determined by direct-shear testing. The measured average peak friction angles were  $36^\circ$  and  $42^\circ$  for the loose and dense sands, respectively.

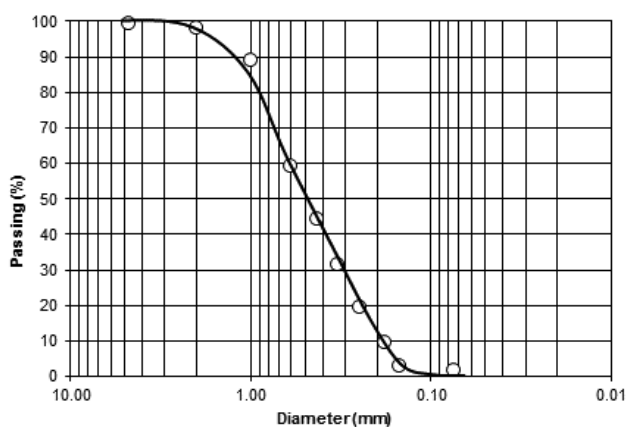


Figure 3. Particle size distribution of test sand.

Table 1. Properties of sand beds.

Property	Value
Coarse sand fraction (%)	0.00
Medium sand fraction (%)	65.00
Fine sand fraction (%)	35.00
$D_{10}$ (mm)	0.16
$D_{30}$ (mm)	0.28
$D_{60}$ (mm)	0.58
Uniformity coefficient, $C_u$	3.63
Coefficient of curvature, $C_c$	0.84
Specific gravity	2.75
Maximum dry unit weight ( $\text{kN/m}^3$ )	17.11
Minimum dry unit weight ( $\text{kN/m}^3$ )	15.44
Dry unit weight of loose sand ( $D_r=25\%$ ) ( $\text{kN/m}^3$ )	15.84
Dry unit weight of dense sand ( $D_r=75\%$ ) ( $\text{kN/m}^3$ )	16.65
Cohesion, $c$ (kPa)	0.00
The angle of shearing resistance of the sand, $\phi$ (degrees)	
Loose sand	36.00
Dense sand	42.00
Classification (USCS)	SP

Note: USCS = Unified Soil Classification System

## 2.3 MODEL FOOTINGS AND TEST TANK

Loading tests were carried out using a model rigid footing fabricated from mild steel, with a thickness of 15mm. The footing had a length of 30cm and a width

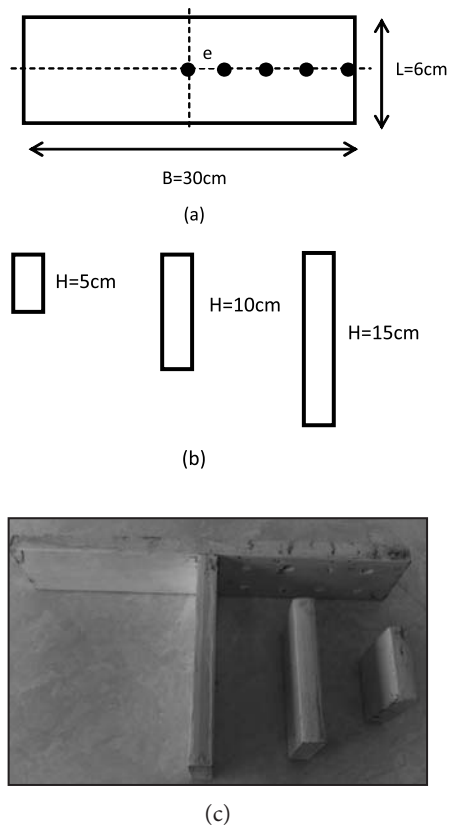


Figure 4. Strip footings: (a) plan view; (b) elevation; (c) photograph.

of 6cm. Figure 4 shows the geometry and the loading system of the model multi-edge footings considered in this investigation. The insertion depths are changed as 5, 10 and 15cm. The same footing ( $L=6\text{cm}$  and  $B=30\text{cm}$ ) was used and only the additional parts were assembled, respectively. The model test configurations were performed both for the loose and the dense sands.

Tests were conducted in a steel tank with dimensions of 0.7m (length), 0.5m (width) and 0.5m (depth). The bottom and vertical edges of the tank were stiffened using angle sections to avoid lateral yielding during the soil placement and loading of the model footing. The two side walls of the tank consist of 10-mm-thick glass plate and the other sides consist of 3-mm steel plate. Therefore, the inside walls of the tank were smooth enough to minimize the side friction. The boundary distances were greater than the footing length, the width and the depth, and during the tests it was observed that the extent of the failure zones was not more than the footing geometry, and the frictional effect was insignificant to affect the results of the model tests. Static vertical loads were applied to the model foundations using an electrically operated mechanical jack attached to a loading frame

located above the tank. Load and displacement measurements were taken using a pressure cell and two LVDTs installed between the jack and the model footing.

## 2.4 EXPERIMENTAL SETUP AND TEST PROGRAM

The sand bed was prepared up to the base level of the model footings in layers that were 50mm thick. Each layer was compacted by a hand-held vibratory compactor in the dense sand case. After the compaction of each sand layer, the next lift height was controlled using scaled lines on the glass plates of the test pit. After the bed's preparation, the sand was carefully levelled in the areas directly beneath the footing. This was to ensure that the model footing had full contact with the sand and that the load applied to the footing was vertical (normal). The model footing tests were performed with the sand at unit weights of  $15.84\text{kN/m}^3$  and  $16.65\text{kN/m}^3$ . To maintain the consistency of in-place density throughout the test pit, the same compactive effort was applied on each layer. The difference in the measured densities was found to be less than 1%. In all the tests the minimum depth of sand below the base of the model was 0.45 m. After the completion of each test, the test pit was excavated to a depth of  $1.5B$  beneath the footing. This depth was chosen since the stress distribution calculated from the PLAXIS-2D computer program [17] dissipates to effectively zero at a depth of about  $1.5B$  below the footing. That means that after the test was completed, only about the last 10 cm remained in the test box.

The model footing was placed on the surface of the sand bed at predetermined locations in the test pit. The vertical compressive load was gradually applied to the model footing by means of a mechanical jack supported against a reaction beam. Then the load was measured using a calibrated pressure cell. A ball bearing was positioned between the proving ring and the footing model to ensure that no extraneous moment was applied to the footing. A constant load increment was maintained until the footing settlement had stabilised. Settlements of the footing were measured using two calibrated LVDTs (Novotechnik TYP TR 50) placed on either side of the footing, as shown in Figure 2. For each test, the load-settlement readings were recorded with a sixteen-channel data-logger unit (MM700 series Autonomous Data Acquisition Unit) and converted to produce values of the settlement at ground level and load using Geotechnical Software-DS7 on a PC. The tests were continued until the applied vertical load was clearly reduced or a considerable settlement of the footing resulted from a relatively small increase in the vertical load. At the end of each test, the sand was carefully excavated.

**Table 2.** Details of model tests.

Test / Analysis Series	Soil Condition	Load Eccentricity	Insertion Depth	Number of Test or Analyses
I	Loose Dense	$e = 0 ; 0.1B ; 0.2B ; 0.3B ; 0.4B ; 0.5B$	$H = 0$	12
II	Loose Dense	$e = 0 ; 0.1B ; 0.2B ; 0.3B ; 0.4B ; 0.5B$	$H = 0.17B ; 0.33B ; 0.50B$	36

In this study, two series of experimental tests and numerical analyses were conducted on the T-shaped model footings. The details are given in Table 2.

### 3 FINITE-ELEMENT ANALYSIS

Numerical analysis is a powerful mathematical tool that makes it possible to solve complex engineering problems. The finite-element method is a well-established numerical analysis technique used widely in many civil-engineering applications, both for research and the solution of real engineering problems. The constitutive behaviour of the soils can be successfully modelled with numerical analyses. The finite-element method is one of the mathematical methods in which continuous media is divided into finite elements with different geometries. It provides the advantage of idealizing the material behaviour of the soil, which is non-linear with plastic deformations and is stress-path dependent, in a more rational manner. The finite-element method can also be particularly useful for identifying the patterns of deformations and stress distribution during deformation and at the ultimate state. Because of these capabilities of the finite-element method, it is possible to model the construction method and investigate the behaviour of shallow footings and the surrounding soil throughout the construction process, not just for the limit equilibrium conditions [18].

Numerical analyses were conducted using the program Plaxis 2D-V2011. It is a finite-element package that is specially developed for the analysis of deformation and stability in geotechnical engineering problems [17]. The stresses, strains and failure states of a given problem can be calculated.

The computer program used in this study incorporates a fully automatic mesh-generation procedure, in which the geometry is divided into elements of the basic element type, and compatible structural elements. Five different mesh densities are available in Plaxis, ranging from very coarse to very fine. In order to obtain the most suitable mesh for the present study, preliminary computations using the five available levels of global mesh coarseness

were conducted. Since there is not too much difference in the results for different mesh configurations, it was decided to use the fine mesh with a refinement around the footing in all the analyses. Plaxis generates full fixity at the base of the geometry and smooth conditions for the vertical sides, including the symmetric boundary. The modelled boundary conditions were assumed such that the vertical boundaries are free vertically and constrained horizontally, while the bottom horizontal boundary is fixed in both the horizontal and vertical directions. The soil medium was modelled using 15-node triangular elements. A typical graded finite-element mesh composed of the soil and footing, together with the boundary conditions and the geometry of the soil system used, is shown in Figure 5.

An elasto-plastic hyperbolic model called the hardening-soil model (HSM) was selected for the non-linear sand behaviour in this study. The HSM is an advanced model for simulating the behaviour of different types of soil, both soft and stiff. The HSM is formulated in the framework of the classical theory of plasticity and supersedes the hyperbolic model: first by using the theory of plastic-

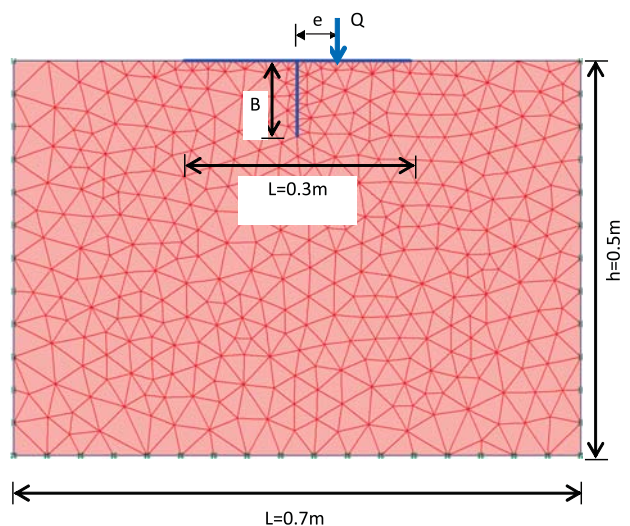


**Figure 5.** Typical mesh configurations in the numerical analyses.

ity rather than the theory of elasticity, second by including soil dilatancy, and third by introducing a yield cap [19]. The model T-shaped footing is modelled as a rigid plate, and is considered to be very stiff and rough in the analyses. Values of the Young's modulus and a Poisson's ratio of  $207 \times 10^6$  kPa and 0.25, respectively, were assumed for the T-shaped footing. The number of triangular elements and nodal points varied with footing geometry arrangements, but the average numbers of triangular elements and nodal points in the mesh were 700 and 6000, respectively. The soil parameters in Table 3 represent the loose and dense sand used in the tests. Brinkgreve et al. [20] reported the following equations for calculating the HSM parameters. In the numerical parts of this study, the parameters for the sand soil were obtained using these equations.

$$E_{50}^{ref} = E_{oed}^{ref} = 6000 \cdot RD / 100 \quad (1)$$

$$E_{ur}^{ref} = 18000 \cdot RD / 100 \quad (2)$$

$$m = 0.7 - RD / 320 \quad (3)$$

$$R_f = 1 - RD / 800 \quad (4)$$

where  $E_{50}^{ref}$ ,  $E_{oed}^{ref}$ ,  $E_{ur}^{ref}$  are the stiffness parameters,  $RD$  is the relative density,  $m$  is the rate of the stress dependency. These parameters are proposed for considering,  $p^{ref} = 100 \text{ kPa}$ .

## 4 RESULTS AND DISCUSSION

### 4.1 GENERAL

Generally, the type of failure in sandy soil was observed as general shear failure. In this type of failure a peak value of  $Q_u$  is clearly defined in the curve of settlement against load (Figure 6).

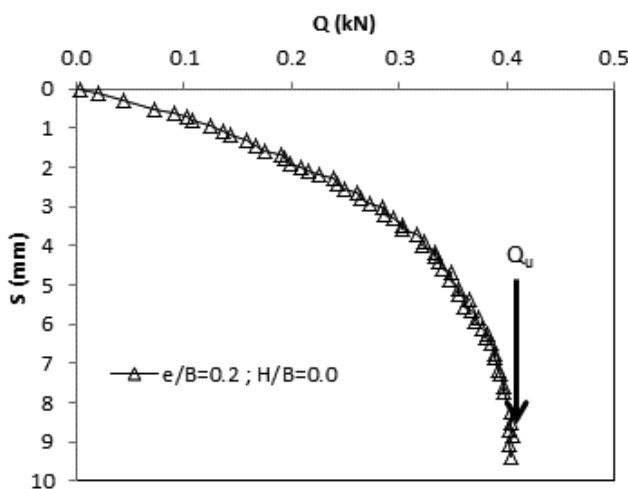


Figure 6. General shear failure.

Table 3. Model parameters for loose and dense sand soils.

HSM Parameters	Loose Sand	Dense Sand
$p^{ref}$ (kPa)	100	100
$\gamma_n$ (kN/m <sup>3</sup> )	15.84	16.65
$E_{50}^{ref}$ (kPa)	15000	45000
$E_{ur}^{ref}$ (kPa)	45000	135000
$E_{oed}^{ref}$ (kPa)	15000	45000
$m$	0.622	0.698
$c$ (kPa)	0.1	0.1
$\phi$ (°)	36	42
$\Psi$ (°)	6	12
$\nu$	0.20	0.20
$K_0$	0.35	0.35
$R_f$	0.969	0.906

### 4.2 SERIES I: EFFECT OF LOAD ECCENTRICITY

Experimental and numerical studies were performed to investigate the effect of load eccentricity on the loose and the dense sand. A total of 12 tests and analyses were carried out using five different footing load eccentricities from  $e/B=0.1$  to 0.5 and including the centric loading. The strip footing used in this series has a width of 0.3 m and length of 0.06 m (Figure 4). The load-settlement and bearing capacity-settlement curves of the loose sand case for different  $e/B$  ratios including centric loading are given in Figure 7. As seen from the figure the loads decrease with an increase in the load eccentricity. The settlement changes presented in Figure 7b are non-dimensional. The settlement ratio ( $S/L$ ) is defined as the ratio of footing settlement ( $S$ ) to footing length ( $L$ ). Similar to the  $Q$ - $S$  relations, the bearing capacity values decrease when the eccentricity ratio increases. For the case of  $e/B > 0.3$ , there is a dramatic decrease in the bearing capacity. Two examples for the loose sand ( $e/B=0$  and  $e/B=0.2$ ) are presented for a comparison of the experimental and numerical results in Figure 8. It is clear from the figure that the vertical displacements predicted by the numerical analysis are in good agreement with the experimental results for the centric loadings and an underestimation is observed for the eccentric loadings.

The relationships between the load-eccentricity ratio ( $e/B$ )-ultimate load ( $Q_u$ ) and the load-eccentricity ratio ( $e/B$ )-ultimate bearing capacity ( $q_u$ ), including the numerical results, are shown in Figure 9. The plots are given for both loose and dense sand. It is clear that the  $Q_u$  and the  $q_u$  values decrease with an increase in the load eccentricity in both the loose and

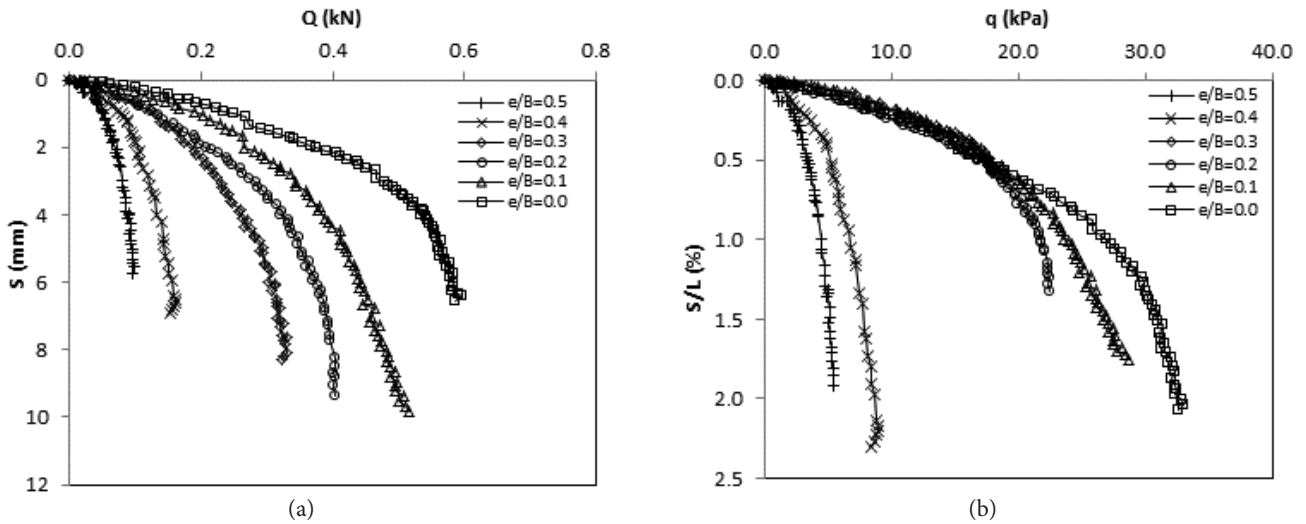


Figure 7. Load-settlement curves for load eccentricity ( $H/B=0$ ).

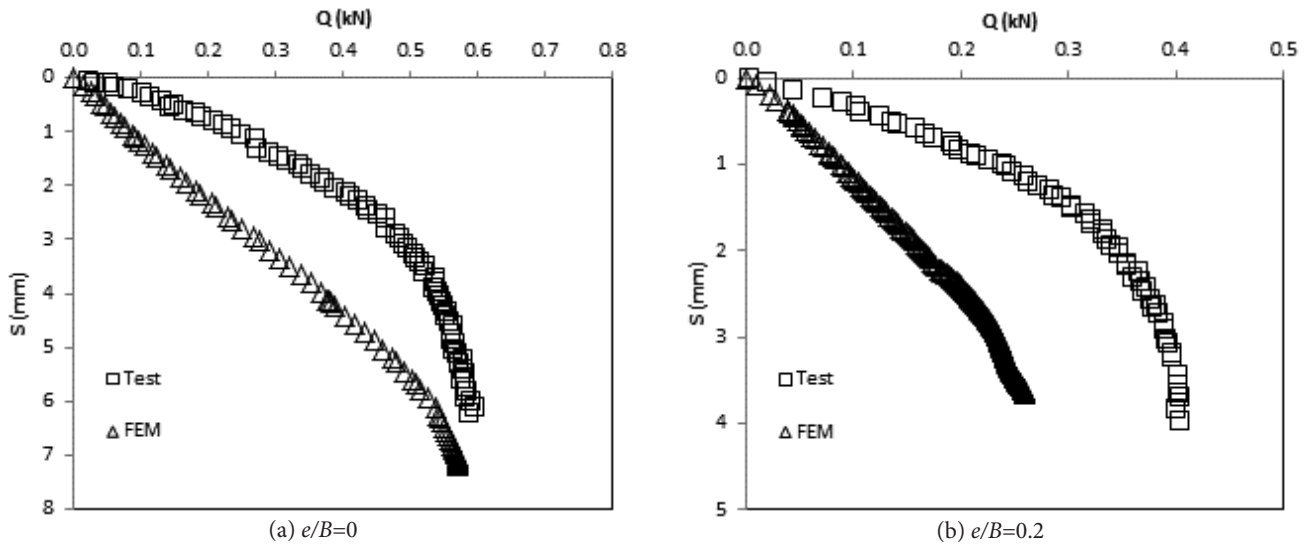


Figure 8. Comparison of test and numerical results for Series I.

dense sands. The test and numerical outcomes confirm the results from the literature [2; 4]. While the load eccentricity increases from 0 to 0.5, the ultimate load decreases by about 83% and 94% in loose and dense sands, respectively. For the same eccentricity ratio, the ultimate bearing capacity decreases by about 5.5 times and 16 times in loose and dense sand, respectively. For the numerical plots, similar behaviour was observed in both the loose and dense sands. The formation in the failure of eccentric footing occurs mainly at one side of the footing, in contrast to the symmetrical failure surfaces at both sides of the footing. This type of failure

mechanism for the eccentric footing loading was observed by many researchers [21–24]. Consequently, this failure mechanism causes less failure surface in the case of the eccentric footing than the same centric footing, since the ultimate load can be regarded as an effort to shear the soil mass along the potential failure surfaces. Due to the eccentric loading, the two edges settle by different amounts, causing the footing to tilt and the pressure below the footing does not remain uniform. The amount of tilt and the pressure at the base depend on the value of the eccentricity-width ratio.



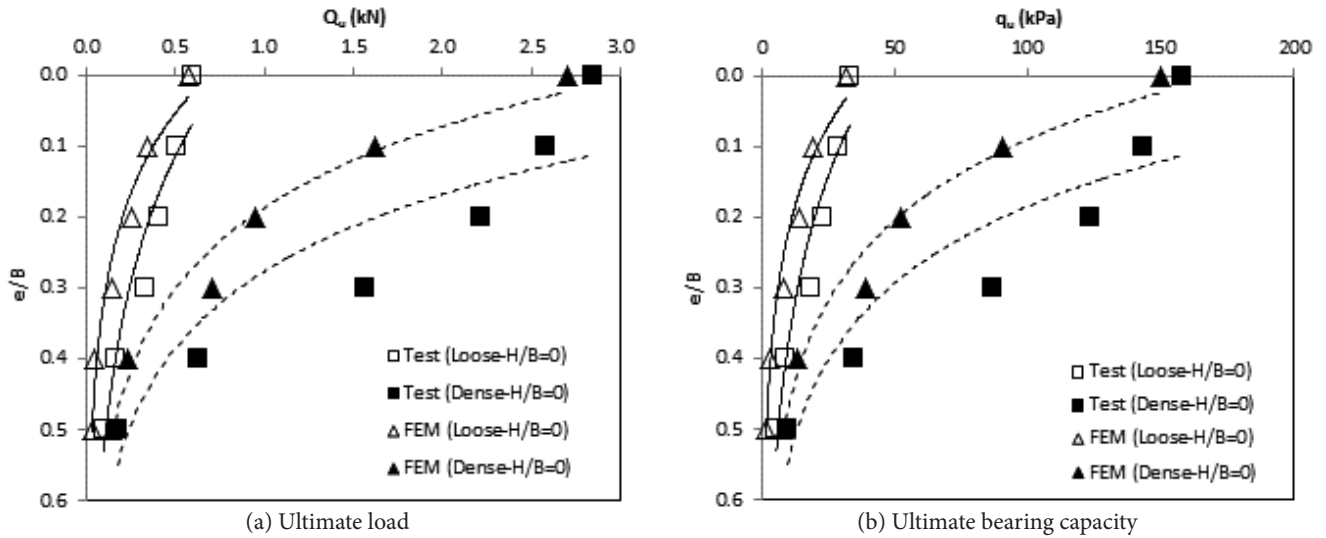
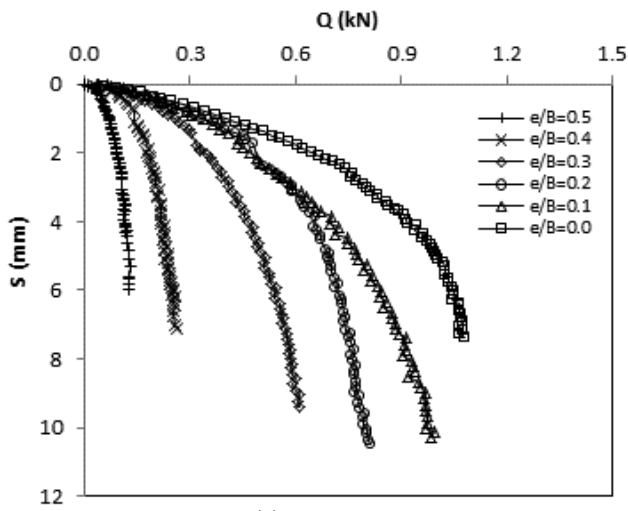
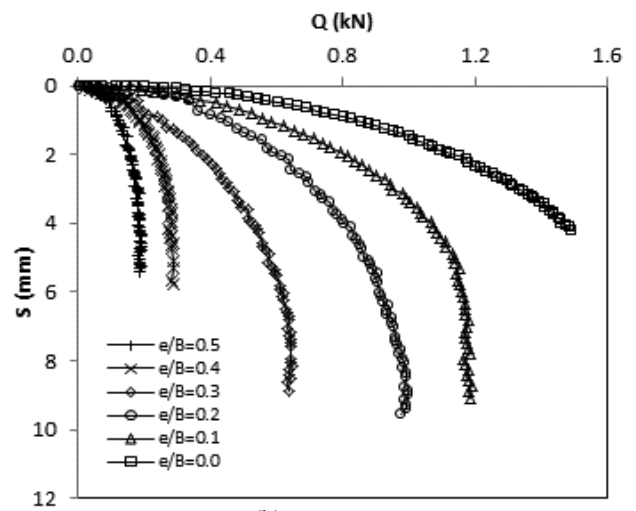


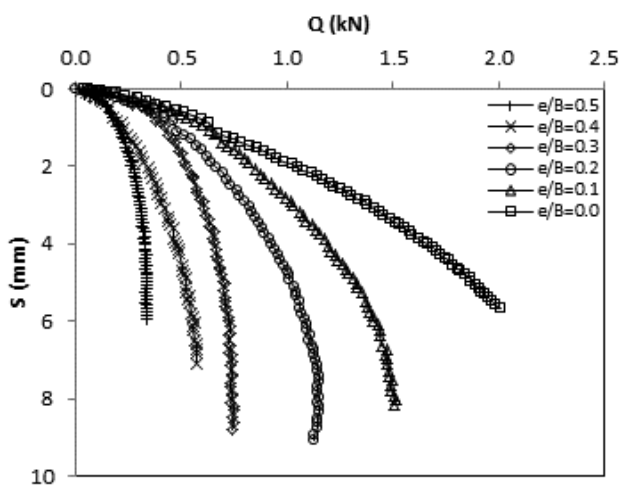
Figure 9. Effect of load eccentricity ( $H/B=0$ ).



(a)  $H/B=0.17$



(b)  $H/B=0.33$



(c)  $H/B=0.50$

Figure 10. Load settlement curves for different insertion depths.

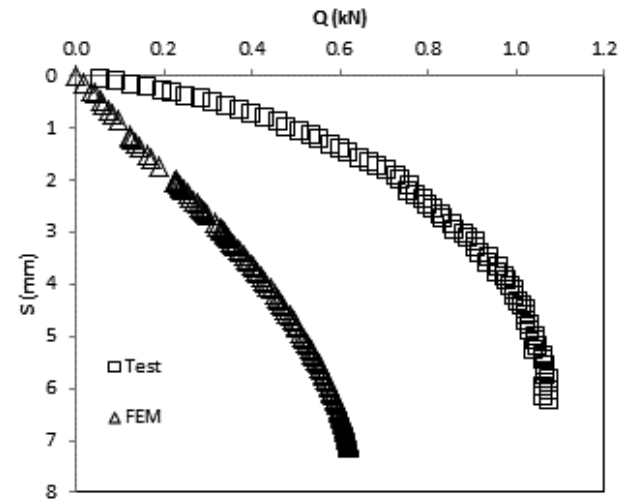
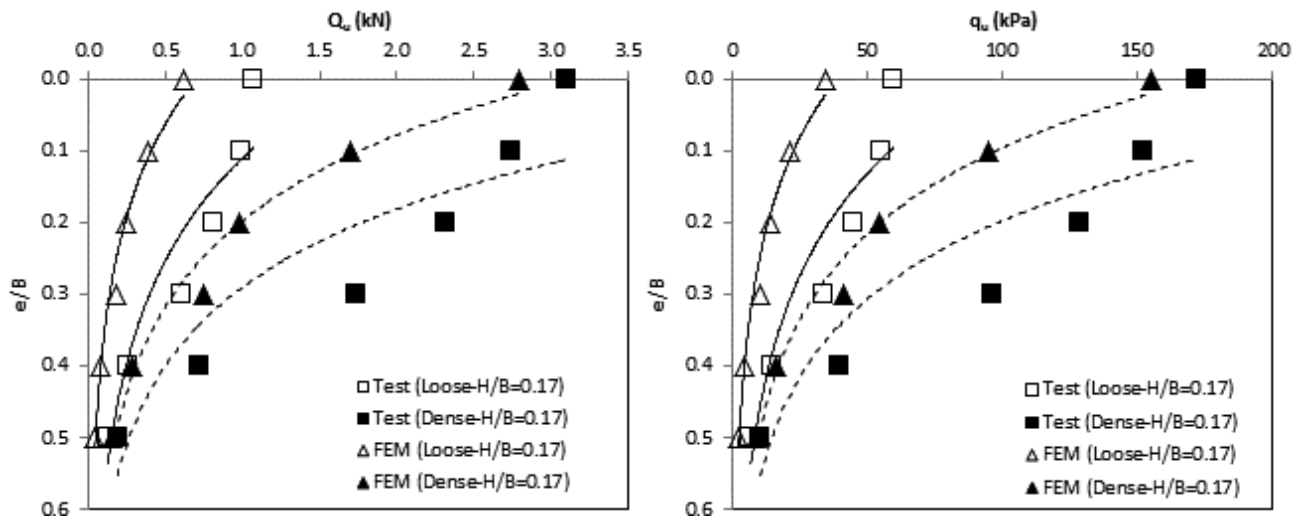
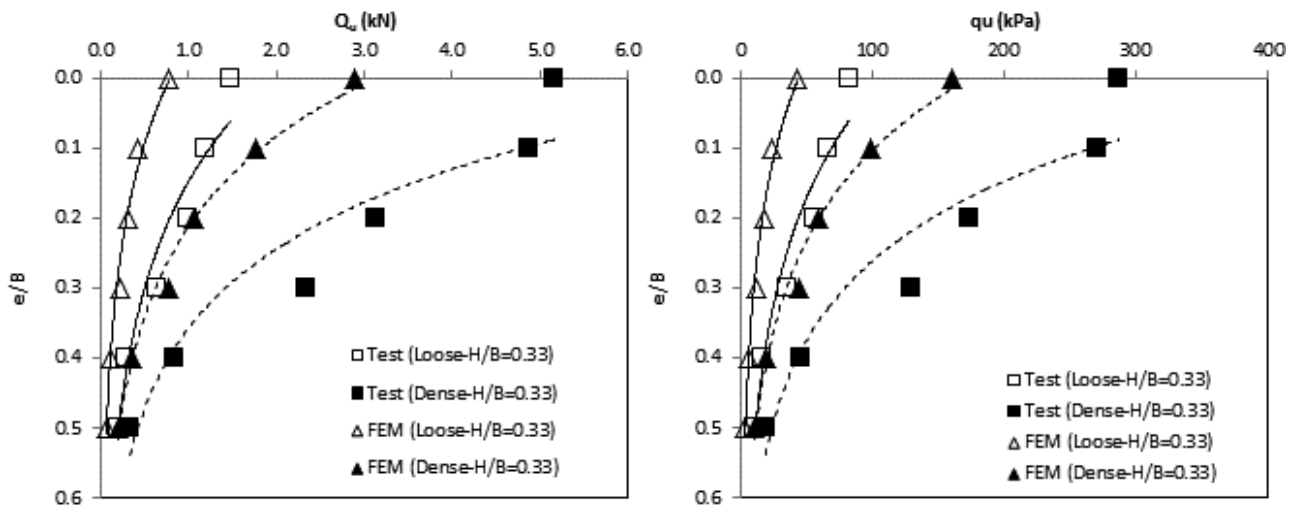


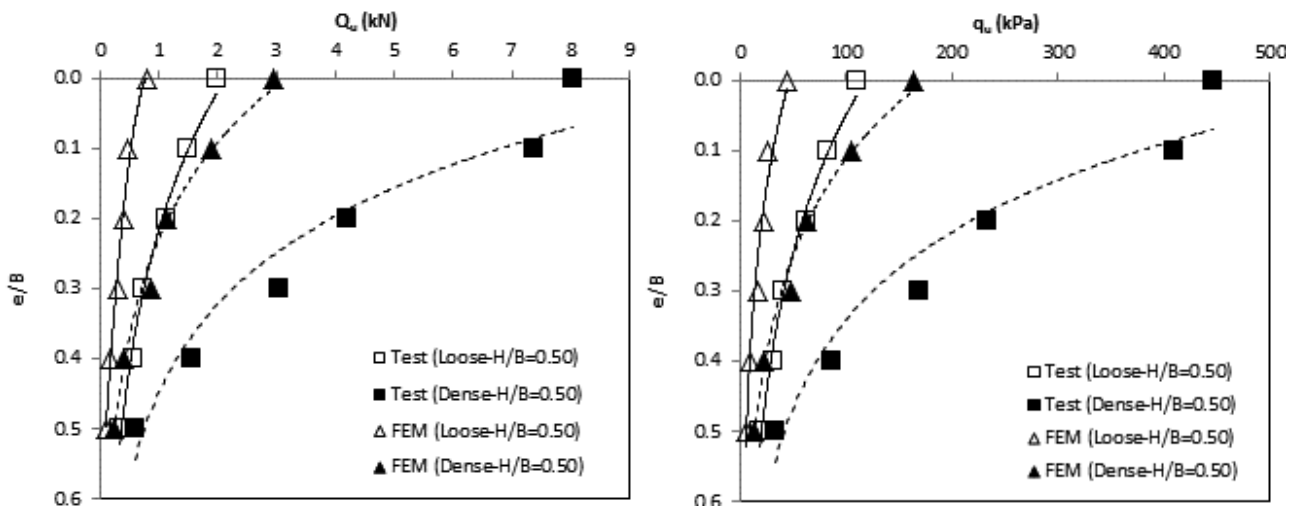
Figure 11. Comparison of test and numerical results for Series II.



(a)  $H/B=0.17$



(b)  $H/B=0.33$



(c)  $H/B=0.50$

Figure 12. Ultimate values for different insertion depths.

### 4.3 SERIES II: EFFECT OF INSERTION DEPTH

In the previous series, the effect of eccentricity was examined. In this series (Series II), the disadvantages of the eccentricity are reduced or eliminated. For this purpose, the rigid T-shaped footing is inserted vertically into the bearing soil. This additional inserted part of the footing provides considerable resistance, against both the sliding and overturning, enough to regain a reduction in the bearing capacity and an increase in the settlement. A total of 36 tests and analyses were performed using three different insertion depths ( $H$ ) of 5 cm, 10 cm, 15 cm and five different load eccentricities namely  $e/B=0.1, 0.2, 0.3, 0.4$  and  $0.5$ , including the centric loading (i.e.,  $e/B=0.0$ ). The same footing ( $L=6\text{cm}$  and  $B=30\text{cm}$ ) is used and only the additional parts are assembled, respectively. The tests

and analyses are performed for both the loose and the dense sand conditions. Figure 10 shows the load-settlement plots for the inserted depths of  $H=0.17B, 0.33B$  and  $0.50B$  under the loose sand case. As seen from the figures, it is clear that the carrying loads decrease with an increase in the load eccentricity. It is also concluded that the depth-inserted part of the T-shaped footing has an important effect on the load-carrying capacity. For the same eccentricity ratio, the load increases when the inserted depth increases.

An example for the loose sand ( $H=0.17B-e/B=0$ ) is presented for a comparison of the experimental and numerical results in Figure 11. Despite there being a similar tendency, the vertical displacements are underestimated by the numerical analysis when compared with the experimental results.

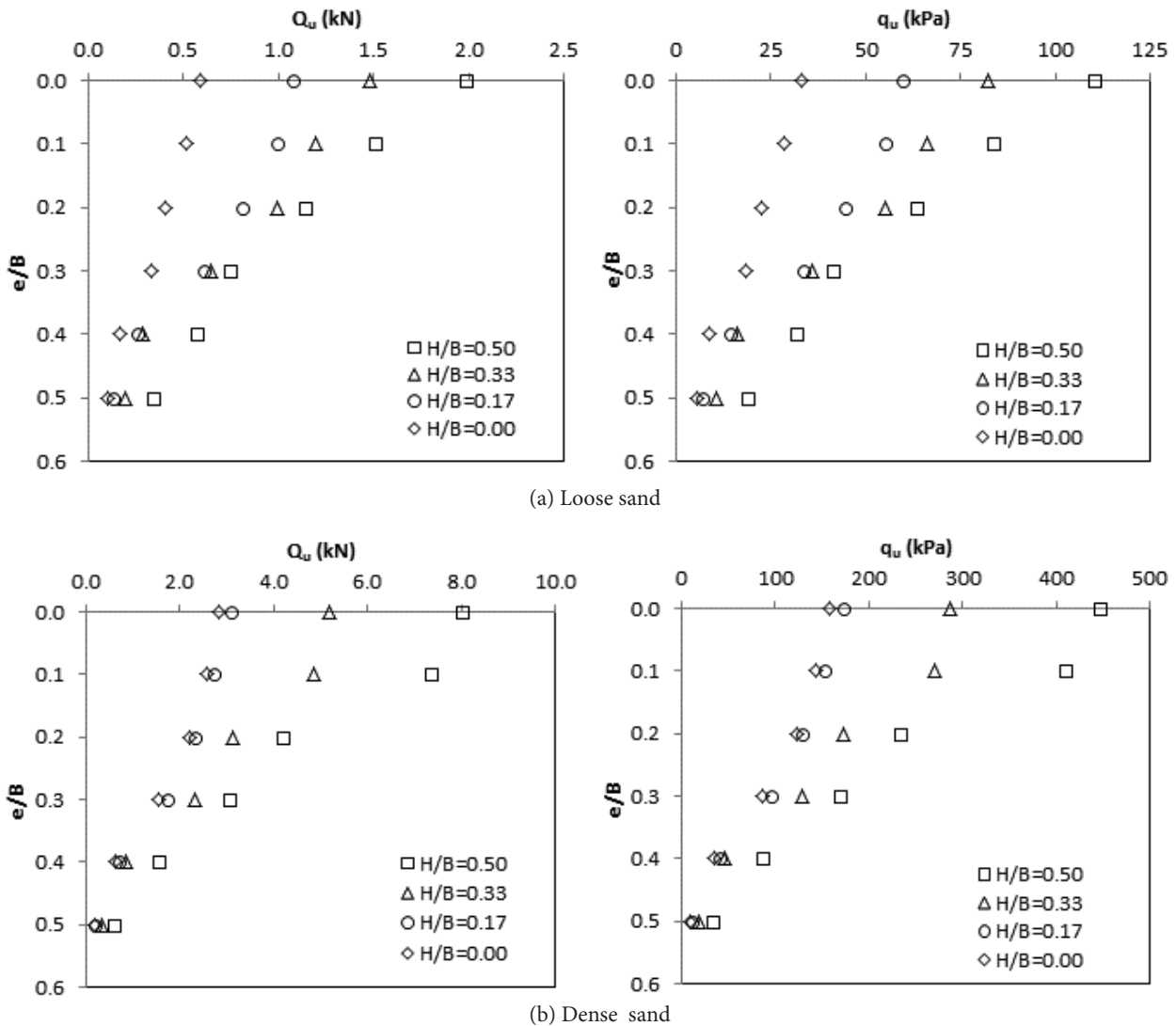


Figure 13. Effect of the insertion depths on the different soil densities.

The ultimate load ( $Q_u$ ) and the ultimate bearing capacity ( $q_u$ ) changes for the different  $e/B$  ratios, including the numerical results, are shown in Figure 12. These relations are presented for each  $H/B$  ratio and for both loose and dense sands. As seen from Figure 12 the ultimate values of  $Q_u$  and  $q_u$  decrease with an increase in the eccentricity ratio,  $e/B$ . Also, for the same eccentricity ratio, these ultimate values increase when the sand gets denser. It is expected that  $Q_u$  and  $q_u$  reach their maximum values at centric loading (i.e.,  $e/B=0$ ) both for loose and dense sand. From the lines in Figure 12a the ultimate load decreases about 16 times when the load eccentricity ratio increases from 0 to 0.5 for the dense sand. The similar logarithmic curves were obtained especially for the cases of  $H=0.33B$  and  $H=0.50B$ . From the plots in Figure 12, similar tendencies are observed between the test and the numerical results. Generally, the finite-element method underestimates the ultimate values obtained from the experimental studies for both the loose and dense sands.

Figure 13 presents the  $Q_u$  and  $q_u$  relations with  $e/B$  ratios using another point of view. The plots are given for both loose and dense sands. As shown in the figures, the ultimate value increases when the insertion depth increases for each eccentric and centric loading. For example, for the loose sand under centric loading, the  $q_u$  value increases from 60kPa to 110kPa when the  $H$  value increases from  $0.17B$  to  $0.50B$ . When the load is applied eccentrically (for example,  $e=0.1B$ , loose sand) the  $q_u$  values calculated are 55kPa and 84kPa for the  $H$  values  $0.17B$  and  $0.50B$ , respectively. Similar behaviour is observed for both the loose and dense sands.

The effect of the inserted depth on the carrying load for the loose sand is investigated for the same eccentric ratio, in Figure 14. The graphs are given for the centric loading ( $e/B=0.0$ ) and the eccentric loading (here,  $e=0.2B$  is selected) conditions. As shown in the figures, the load increases when the insertion depth increases. The same phenomenon is observed for both the centric and eccentric loading conditions. For a constant settlement value, such as 5 mm, the measured centric loads are 0.56kN, 1.05kN, 1.44kN and 1.92kN, for  $H=0$ ,  $H=0.17B$ ,  $H=0.33B$  and  $H=0.50B$ , respectively. Similarly, for the eccentric loadings, the measured values considering the settlement of 2.5 mm are 0.38kN, 0.78kN, 0.99kN and 1.15kN. There is also a difference in the settlement values for the centric and the eccentric loading cases. On the other hand, the effect of the eccentricity (as discussed earlier) is easily seen from the plots.

The expected failure patterns under the eccentric loading conditions are discussed in Figure 15. As investigated in Figure 15a, under the action of a vertical eccentric load ( $Q$ ), the footing is settled vertically as  $S$ , and rotates with a definite rotation angle. When the failure stage occurs or the carrying load exceeds the ultimate value, a one sided failure pattern will occur in the soil, as pointed out in Figure 15b. Due to the rotation component, the bearing capacity is dramatically decreased, so that, preventing the rotation could help in improving the carrying capacity of the footings. Therefore, a T-shaped footing is used to improve the bearing capacity of these footings against the action of the eccentric loads. Figure 15c shows this mechanism, i.e., the failure pattern of a T-shaped footing under the eccentric loading. In this mechanism, rotation prevention could be attributed to the resistance of the created additional passive zone. It is observed from the experimental results that with the increase in the insertion depth ( $H$ ), the rotation could be prevented.

The finite-element method generates an effective analysis and evaluation of the displacements, stresses and forces in and around the soil, the stabilized bodies and the

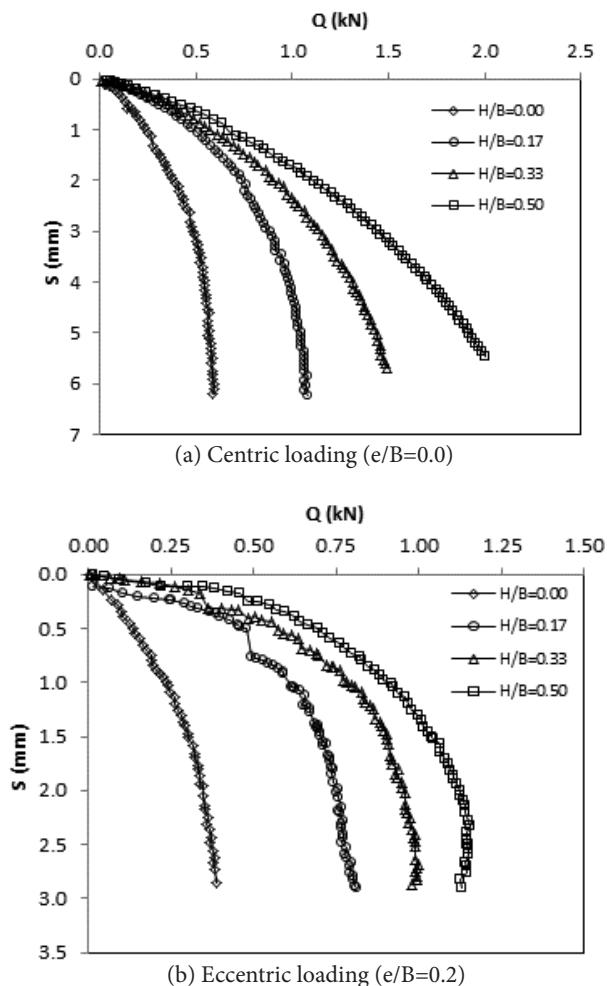


Figure 14. Effect of the insertion depths on the loading conditions.

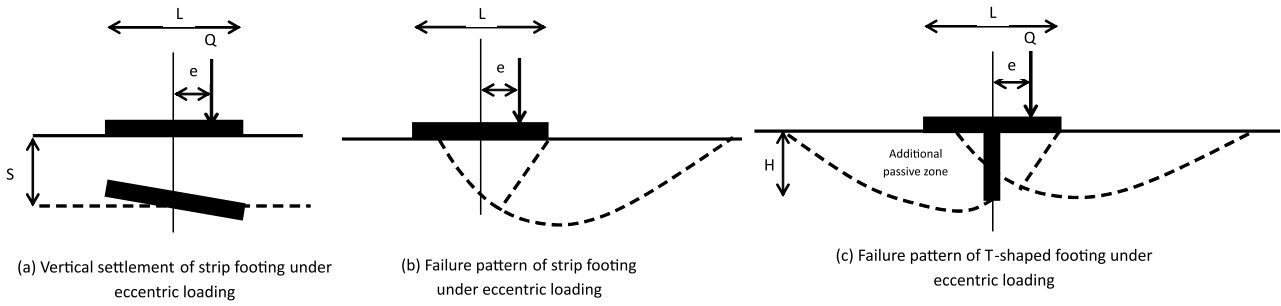


Figure 15. Collapse mechanism.

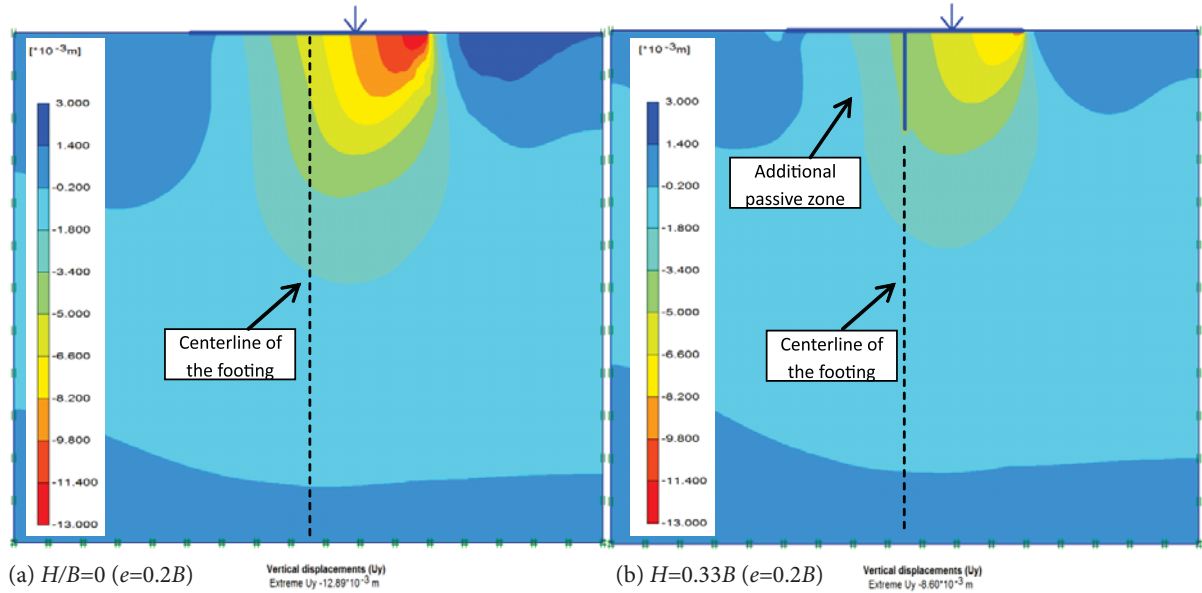


Figure 16. Vertical displacement fields below the T-shaped footings.

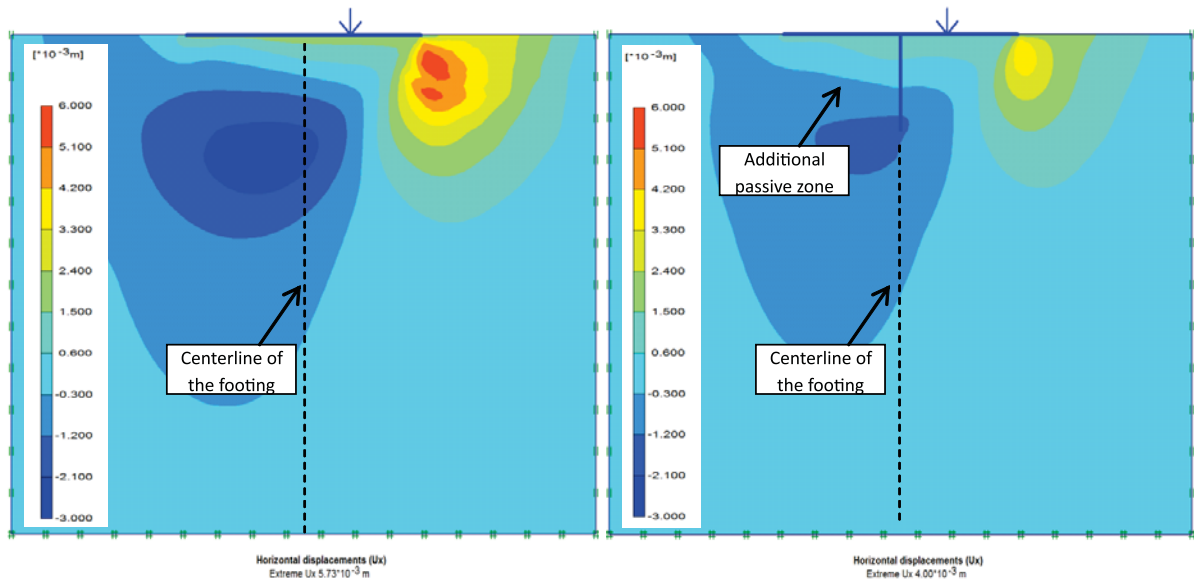


Figure 17. Horizontal displacement fields below the T-shaped footings.

footing. Figures 16 and 17 show some typical examples of the resultant vertical and horizontal displacement fields below the strip footing ( $H/B=0$ ,  $e=0.2B$ ) and the T-shaped footing cases ( $H=0.33B$ ,  $e=0.2B$ ) at the failure load of the strip footing. It can be seen that there is a clear reduction in the vertical and horizontal displacements for the T-shaped footing case compared with the strip footing case. A similar mechanism to that described in Figure 15 is observed numerically. In this mechanism, with the increase in the insertion depth ( $H$ ), the rotation could be prevented. As seen from Figure 16, the maximum vertical displacement below the T-shaped footing decreases from  $12.89 \times 10^{-3}$  m to  $8.60 \times 10^{-3}$  m when the footing is supported by an insertion. In a similar manner, the maximum horizontal displacement values are  $5.73 \times 10^{-3}$  m and  $4.00 \times 10^{-3}$  m. The insertion part prevents the rotation of the footing by the additional passive zone.

Figure 18 shows the changes in the settlements along the length of the four different types ( $H/B$  ratio changes from 0 to 0.50) of footings. An eccentricity ratio of 0.2 is chosen. The horizontal axis represents the distances along the footings. The zero point refers to the centre of the footings. The settlement along the depth is seen in the vertical axis. These numerical data were obtained for the ultimate load of  $H/B=0$ - $e/B=0.2$ , i.e., for the strip footing condition. As seen from these numerical data, the settlement decreases when the  $H/B$  ratio increases. It is clear that there are heave zones in the

sand soil, well away from the application point of the load.

The maximum value for each footing type is obtained beneath the loading point. Similar findings were also obtained in the tests and the heave zones were visually observed.

## 5 LIMITATIONS

There are several limitations that should be mentioned. It is well known that full-scale loading test results are valid, especially for in-situ conditions and for soil properties in which the test was performed. However, a full-scale loading test is not economic, due to the expensive cost in terms of time and money that is required for the construction, instrumentation and testing. Therefore, small-scale model test studies are widely used as an alternative to full-scale loading tests, despite of their scale-errors [25]. Then, the tests were conducted on only one soil type. The results observed from this test program may be different for other soils. Additionally, only the model tests were introduced. The numerical analyses can also be included in future works, after some validation processes. The additional research using T-shaped footings with an angle and different geometries and soil beds is recommended as further investigations to improve the understanding of the bearing capacity and the settlement behaviour comprehensively, which may lead to developing a design method.

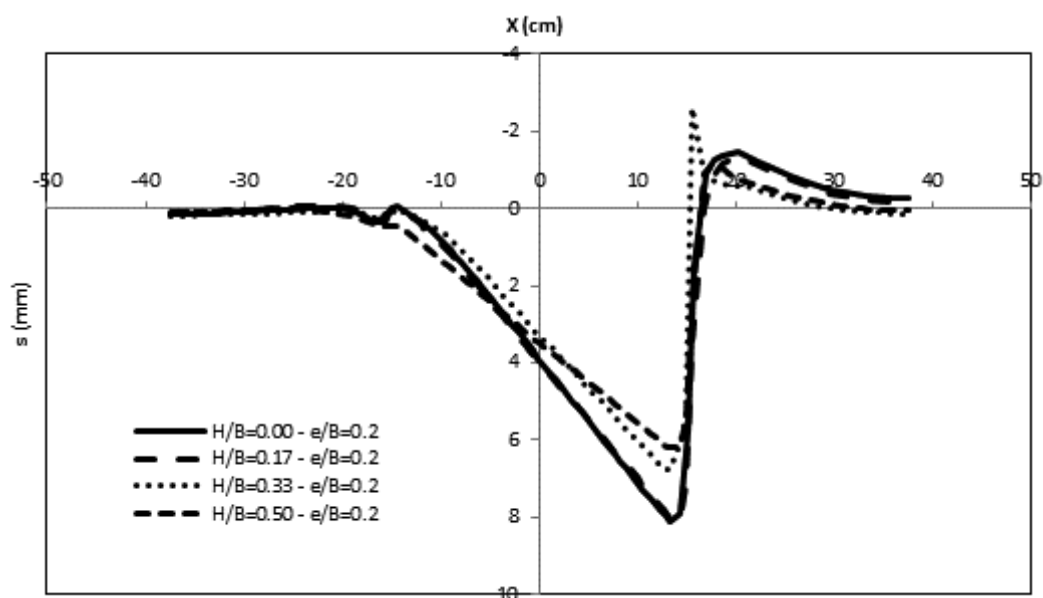


Figure 18. Settlement changes below the footings.

## 6 CONCLUSIONS

In this study, experimental and numerical investigations into the ultimate loads of T-shaped footings are reported. The effect of eccentricity and the effect of the insertion depths under vertical loadings were investigated in Series I and Series II, respectively. The studies in every test series were performed for both loose and dense sand conditions. At the end of the test and the numerical analysis, the load-settlement and bearing capacity-settlement curves were plotted. Based on the results of this investigation, the following main conclusions can be drawn:

- It is observed that the carrying loads and the bearing capacity of the strip footing decrease with an increase in the load eccentricity for both the loose and dense sands. There is a dramatic decrease in the bearing capacity, especially for the case of  $e/B > 0.3$ . The formation in the failure of the eccentric footing occurs mainly at one side of the footing, in contrast to the symmetrical failure surfaces on both sides of the footing.
- The ultimate loads and the ultimate bearing capacity values decrease with an increase in the load eccentricity. While the load eccentricity increases from 0 to 0.5, the ultimate loads decrease by about 83% and 94% in the loose and dense sand, respectively. For the same eccentricity ratios, the ultimate bearing capacity decreases about 5.5 times and 16 times in the loose and dense sand, respectively.
- The depth of the inserted part of the T-shaped footing has an important effect on the load-carrying capacity. For the same eccentricity ratio, the carrying load increases when the inserted depth increases.
- Similar to the strip footings, the ultimate values of the loads and the ultimate bearing capacities decrease with the increase in the eccentricity ratios for the T-shaped footings. And also, for the same eccentricity ratio, these ultimate values are increased when the sand gets denser.
- The ultimate loads and the ultimate bearing capacities reach their maximum values for the centric loading (i.e.,  $e/B=0$ ) both for loose and dense sand. The ultimate load decreases about 16 times when the load eccentricity ratio increases from 0 to 0.5 for the dense sand for the case of  $H=0.17B$ .
- The ultimate values increase when the insertion depth increases. For the loose sand under centric loading the  $q_u$  value increases from 60kPa to 110kPa when the  $H$  value increases from  $0.17B$  to  $0.50B$ . When the load applied eccentrically (for example,  $e=0.1B$ ) the  $q_u$  value increases are calculated as 55kPa and 84kPa for the  $H$  values  $0.17B$  and  $0.50B$ . Similar

behaviour is observed both for the loose and dense sands.

- Numerical analyses, using an elasto-plastic hyperbolic model (Hardening Soil Model), gave results that have a similar tendency to those from physical model tests. Generally, the numerical model used in the analyses underestimates the test results. This means more conservative results are obtained with the numerical analyses.

Nevertheless, the investigation is considered to have provided a useful basis for further research leading to an increased understanding of the application of T-shaped footings to the ultimate bearing capacity and settlement problems.

## REFERENCES

- [1] Patra, C.R., Das, B.M., Bhoi, M. and Shin, E.C. (2006). Eccentrically loaded strip foundation on geogrid-reinforced sand. *Geotextiles and Geomembranes*, Vol. 24, No. 4, pp. 254–259.
- [2] Singh, V.K., Prasad, A. and Agrawal, R.K. (2007). Effect of soil confinement on ultimate bearing capacity of square footing under eccentric–inclined load. *EJGE*, Vol. 12, Bund E.
- [3] Saleh, N.M., Alsaied, A.E. and Elleboudy, A.M. (2008). Performance of skirted strip footing subjected to eccentric inclined load. *EJGE*, Vol. 13, Bund F.
- [4] Sadoglu, E., Cure, E., Moroglu, B. and Uzuner, B.A. (2009). Ultimate loads for eccentrically loaded model shallow strip footings on geotextile-reinforced sand. *Geotextiles and Geomembranes*, Vol. 27, No. 3, pp. 176–182.
- [5] Joshi, D.P. and Mahiyar, H.K. (2009). Effectiveness of angle shaped footings resting on soil under eccentric inclined load. *International Journal of Theoretical Applied Mechanics*, Vol. 4, No. 1, pp. 95–105.
- [6] Musso, A. and Ferlisi, S. (2009). Collapse of a model strip footing on dense sand under vertical eccentric loads. *Geotechnical and Geological Engineering*, Vol. 27, No. 2, pp. 265–279.
- [7] Nawghare, S. M., Pathak, S. R. and Gawande, S. H. (2010). Experimental investigations of bearing capacity for eccentrically loaded footing. *International Journal of Engineering Science and Technology*, Vol. 2, No. 10, pp. 5257–5264.
- [8] Taiebat, H.T. and Carter, J.P. (2001). A semi-analytical finite element method for three-dimensional consolidation analysis. *Computers and Geotechnics*, Vol. 28, pp. 55–78.

- [9] Taiebat, H.A. and Carter, J.P. (2002). Bearing capacity of strip and circular foundations on undrained clay subjected to eccentric loads. *Geotechnique*, Vol. 52, No. 1, pp. 61–64.
- [10] Hjiiaj, M., Lyamin, A.V. and Sloan, S.W. (2004). Bearing capacity of a cohesive-frictional soil under non-eccentric inclined loading. *Computers and Geotechnics*, Vol. 31, No. 6, pp. 491–516.
- [11] Saran, S., Kumar, S., Garg, K.G. and Kumar, A. (2007). Analysis of square and rectangular footings subjected to eccentric-inclined load resting on reinforced sand. *Journal of Geotechnical and Geoenvironmental Engineering*, Vol. 25, No. 1, pp. 123–137.
- [12] Loukidis, D., Chakraborty, T. and Salgado, R. (2008). Bearing capacity of strip footings on purely frictional soil under eccentric and inclined loads. *Canadian Geotechnical Journal*, Vol. 45, No. 6, pp. 768–787.
- [13] Srinivasan, V. and Ghosh, P. (2012). Experimental investigation on interaction problem of two nearby circular footings on layered cohesionless soil. *Geomechanics and Geoengineering: An International Journal*, 1–10.
- [14] Veiskarami, M. and Kumar, J. (2012). Bearing capacity of foundations subjected to groundwater flow. *Geomechanics and Geoengineering: An International Journal*, Vol. 7, No. 4, pp. 293–301.
- [15] He, W. (2012). Application of the meshfree method for evaluating the bearing capacity and response behavior of foundation piles. *International Journal of Geomechanics*, Vol. 12, No. 2, pp. 98–104.
- [16] Dash, S. (2012). Effect of geocell type on load-carrying mechanisms of geocell-reinforced sand foundations. *International Journal of Geomechanics*, Vol. 12, No. 5, pp. 537–548.
- [17] Brinkgreve, R.B.J., Swolfs, W.M. and Engin, E. (2011). Plaxis Finite Element Code for Soil and Rock Analysis. *Plaxis 2D 2011*.
- [18] Laman, M. and Yildiz, A. (2007). Numerical studies of ring foundations on geogrid-reinforced sand. *Geosynthetics International*, Vol. 14, No. 2, pp. 52–64.
- [19] Schanz, T., Vermeer, P.A. and Bonnier, P.G. (1999). The hardening soil model: formulation and verification. *Beyond 2000 in Computational Geotechnics*, A. A. Balkema Publishers, Rotterdam, pp. 281–296.
- [20] Brinkgreve, R.B.J., Engin, E. and Engin, H.K. (2010). Validation of empirical formulas to derive model parameters for sands. *Knowledge Base Publications of Plaxis, Plaxis B.V., Delft, Netherlands*.
- [21] Meyerhof, G. G. (1953). The bearing capacity of foundations under eccentric and inclined loads. *In: Proceedings of the Third International Conference on Soil Mechanics and Foundation Engineering*, pp. 440–445.
- [22] Prakash, S. and Saran, S. (1971). Bearing capacity of eccentrically loaded footings. *Journal of SM and FE Division ASCE*, Vol. 97, No. 1, pp. 95–117.
- [23] Uzuner, B.A. (1975). Centrally and eccentrically loaded strip foundations on sand. PhD thesis, Strathclyde University, Glasgow, Scotland.
- [24] Moroglu, B. (2002). The bearing capacity of the eccentrically loaded model strip footing on reinforced sand. PhD thesis, Black Sea Technical University, Turkey.
- [25] Dickin, E.A. and Nazir, R. (1999). Moment-carrying capacity of short pile foundations in cohesionless soil. *Journal of Geotechnical and Geoenvironmental Engineering, ASCE*, Vol. 125, No. 1, pp. 1–10.